Mon. Not. R. Astron. Soc. **000**, 1–12 () Printed 19 February 2024 (MN LATEX style file v2.2)

The disk averaged star formation relation for Local Volume dwarf galaxies

Á. R. López-Sánchez[1,2,3⋆], C.D.P. Lagos[4,5,3], T. Young[2,6,7], H. Jerjen[6]
[1] *Australian Astronomical Observatory, 105 Delhi Road, North Ryde, NSW 2113, Australia*
[2] *Department of Physics and Astronomy, Macquarie University, NSW 2109, Australia*
[3] *Australian Research Council Centre of Excellence for All Sky Astrophysics in 3 Dimensions (ASTRO 3D), Australia*
[4] *International Centre for Radio Astronomy Research (ICRAR), M468, University of Western Australia, 35 Stirling Hwy, Crawley, WA 6009, Australia.*
[5] *Australian Research Council Centre of Excellence for All-sky Astrophysics (CAASTRO), 44 Rosehill Street Redfern, NSW 2016, Australia.*
[6] *Research School of Astronomy and Astrophysics, The Australian National University, Mt Stromlo Observatory, via Cotter Rd, Weston, ACT 2611, Australia*
[7] *CSIRO Astronomy and Space Science, Australia Telescope National Facility, PO Box 76, Epping, NSW 1710, Australia*

arXiv:1805.05003v1 [astro-ph.GA] 14 May 2018

ABSTRACT
Spatially resolved H I studies of dwarf galaxies have provided a wealth of precision data. However these high-quality, resolved observations are only possible for handful of dwarf galaxies in the Local Volume. Future H I surveys are unlikely to improve the current situation. We therefore explore a method for estimating the surface density of the atomic gas from global H I parameters, which are conversely widely available. We perform empirical tests using galaxies with resolved H I maps, and find that our approximation produces values for the surface density of atomic hydrogen within typically 0.5 dex of the true value. We apply this method to a sample of 147 galaxies drawn from modern near-infrared stellar photometric surveys. With this sample we confirm a strict correlation between the atomic gas surface density and the star formation rate surface density, that is vertically offset from the Kennicutt-Schmidt relation by a factor of $10-30$, and significantly steeper than the classical $N = 1.4$ of Kennicutt (1998). We further infer the molecular fraction in the sample of low surface brightness, predominantly dwarf galaxies by assuming that the star formation relationship with molecular gas observed for spiral galaxies also holds in these galaxies, finding a molecular-to-atomic gas mass fraction within the range of 5-15%. Comparison of the data to available models shows that a model in which the thermal pressure balances the vertical gravitational field captures better the shape of the $\Sigma_{\rm SFR}$-$\Sigma_{\rm gas}$ relationship. However, such models fail to reproduce the data completely, suggesting that thermal pressure plays an important role in the disks of dwarf galaxies.

Key words: galaxies: dwarf; galaxies: irregular; galaxies: structure, star formation

1 INTRODUCTION

Star formation, the process by which gas is converted into stars, plays a central role in the evolution of a galaxy. Empirical constraints on the relationships between the present day quantities of gas and star formation in galaxies may therefore form a crucial component in sub-grid recipes of hydrodynamic simulations and semi-analytical models. (e.g. Furlong et al. 2015; Popping, Somerville & Trager 2014; Kuhlen et al. 2012; Lagos et al. 2011; Fu et al. 2010); which trace the formation of baryonic structures (galaxies) in dark matter halos. Attempts to study the relationship between the gas and star formation rate (SFR) have been long standing (Schmidt 1959), however only in modern times could any such relationship be demonstrated (Kennicutt 1998). In his pioneering study, Kennicutt (1998) found a strong correlation between the SFR surface density and the total gas surface density, fitting a power law relation to a sample of spiral and starburst galaxies of the form,

$$\Sigma_{\rm SFR} = A\Sigma_{\rm Gas}^{N}.$$

Power law parametrisations of these quantities are referred to henceforth in this work simply as a star formation re-

⋆ angel.lopez-sanchez@aao.gov.au

lation, or interchangeably, the Kennicutt-Schmidt relation (KS).

More recent studies achieved sufficient sensitivity and angular resolution to study the inner regions of Local Volume (d $\lesssim$ 10 Mpc) spiral galaxies on kpc scales. These resolved studies instead demonstrated strict correlation between the observed surface densities of molecular hydrogen H_2 and the SFR surface density whilst simultaneously demonstrating an anti-correlation with atomic hydrogen (H I) above its saturation limit (Kennicutt et al. 2007; Bigiel et al. 2008; Leroy et al. 2008). These studies indicated that the star formation relation was universal only when considering the molecular gas and not the total gas, for which the derived slope varied within and between galaxies. Indeed Krumholz, McKee & Tumlinson (2009b) successfully derived an universal local star formation relation, with significantly reduced scatter when considering a 'free-fall' time $t_{\rm ff}$

$$\Sigma_{\rm SFR} = f_{H_2} \epsilon_{\rm ff} \frac{\Sigma_{\rm gas}}{t_{\rm ff}}$$

where f_{H_2} is the fraction of the molecular gas and $\epsilon_{\rm ff}$ is a dimensionless star formation efficiency (SFE) scale factor (see Krumholz (2014) for a recent review on the subject). Further studies have challenged the universality of even the molecular star formation relation law (e.g. see discussions by Shetty et al. 2014; Leroy et al. 2013b). Comprehensive theoretical models should therefore accurately describe the observed distribution of apparent gas depletion times as a function of various environmental conditions or other factors and not just simply the surface densities of gas and SF. Comparing the agreement of the available data to theoretical models with varying underlying assumptions will therefore provide greater insight than just examining the linear regressions.

While in the inner disks of Local Volume spirals, the H I content was not found to correlate with SFR surface density, the reverse is true in the outer H I dominated disks and low-mass late type galaxies (Bigiel et al. 2010; Bolatto et al. 2011). Pushing H_2 column densities from 10 $M_{\odot}{\rm pc}^{-2}$ to 1 $M_{\odot}{\rm pc}^{-2}$, Schruba et al. (2011) and Bolatto et al. (2011) showed the molecular surface density still correlated with the SFR surface density. These facts together imply that the molecular fraction in the Interstellar Medium (ISM) reaches a floor value of a few percent (Krumholz 2013). Ostriker, McKee & Leroy (2010) and Krumholz (2013) developed theoretical models in order to describe the levels of star formation observed in the the H I -dominated regime, with varying degrees of success. The Krumholz (2013) model successfully describes the outer disks of spirals and dwarf galaxies (Bolatto et al. 2011; Bigiel et al. 2010; Koribalski & López-Sánchez 2009). However for disk averaged quantities derived from dwarf galaxies (Wyder et al. 2009; Roychowdhury et al. 2014) and the resolved Roychowdhury et al. (2015) data set, the Ostriker, McKee & Leroy (2010) model provides better agreement. A key difference between the two models is that Krumholz (2013) includes the effect of gas metallicity on the transition from atomic to molecular hydrogen, which is inspired by the premise that H_2 forms on the surface of dust grains. The Ostriker, McKee & Leroy (2010) model does not consider the chemical state of the gas, but only its thermodynamic state by imposing pressure balance between the different ISM phases. With different underlying theoretical assumptions, distinguishing between these two models will provide important insight into the processes which govern star formation in H I dominated environments.

While resolved studies of dwarf galaxies have provided a wealth of precision data, taken together, these studies (Roychowdhury et al. 2015; Bigiel et al. 2010) were constrained to only 27 dwarf galaxies of the 107 observed by Hunter et al. (2012) and Begum et al. (2008) compared with the $\sim$ 400 irregular galaxies in the Local Volume. Future H I surveys, whilst very sensitive, are unlikely to resolve anything but the nearest dwarf galaxies (Koribalski 2012, 2008). Despite this, multi-wavelength coverage of dwarf galaxies in the Local Volume is particularly good, (see Karachentsev, Makarov & Kaisina 2013, and references therein), often only the H I resolution is lacking. In order to increase the sample size to include dwarfs at greater distances, we must find approximate methods for computing the surface gas density. In this work, we provide a procedure for approximating the surface density of the gas from global H I parameters and precision stellar photometry. We test the accuracy of our method by using the Wyder et al. (2009) and Kennicutt (1998) galaxies as control samples.

This paper is organised as follows: In Section 2 we describe the galaxy samples, catalogues and our computed parameters. In Section 3 we present our results, analysis and discussion. Particularly, we describe the accuracy of our gas surface density estimation. We then compare our data to resolved observations. Although a vertically offset population to the spirals, we demonstrate that the sample of low surface brightness galaxies, predominantly dwarfs, forms a smooth distribution. Considering only the vertical offset and assuming a constant time-scale to convert the H_2 into star formation, we provide an estimation of a typical molecular fraction. In Section 4 we compare all the available data in the literature to various models. Finally, we conclude in Section 5.

2 METHODOLOGY

2.1 Samples

To study the star formation relation, (from here on we use the phrases star formation relation and the KS relation interchangeably) in a comprehensive sample of Local Volume dwarfs ($M_* < 9\ M_{\odot}$), low-mass late types and low-surface brightness galaxies, we employ data from various sources in the literature which we describe below.

2.1.1 Near-infrared photometry

The global disk-averaged quantities used in the KS relation are typically computed from some fiducial radius corrected for inclination that is ideally representative of the star-forming disk. The choice of radius has not remained consistent over time. The K98 sample parameters were computed using the 'RC2 radius', the B-band 25th surface brightness isophotal diameters from the second reference catalogue (i.e. D_{25}, de Vaucouleurs, de Vaucouleurs & Corwin 1976). Wyder et al. (2009) instead used the circle defined by the semi-major axis of the ellipse used to extract the UV

flux. Roychowdhury et al. (2014) has assumed that the star-forming disk is well described by the ellipse defined by the Holmberg diameter (Holmberg 1958), which corresponds to a B-band isophotal brightness of 26.5 mag arcsec^{-2}, based on morphological comparisons of the FUV, H I and Hα. Photometric studies of nearby galaxies (e.g. Lauberts & Valentijn 1989; de Vaucouleurs et al. 1991; Bremnes, Binggeli & Prugniel 1998, 1999, 2000; Jerjen, Binggeli & Freeman 2000; Barazza, Binggeli & Prugniel 2001; Parodi, Barazza & Binggeli 2002; Makarova et al. 2005) were typically conducted in the optical regime and thus definitions of the stellar and star-forming disks naturally followed from B-band photometry. Improvements in CCD technology and the introduction of near-infrared (NIR) detectors have since resulted in accurate *JHKs* photometery of Local Volume galaxies (e.g., Noeske et al. 2003; Vaduvescu et al. 2005; Vaduvescu, Richer & McCall 2006; Vaduvescu & McCall 2008; Kirby et al. 2008; Fingerhut et al. 2010; de Swardt, Kraan-Korteweg & Jerjen 2010; McCall et al. 2012; Young et al. 2014). In cases where the integration times are sufficient to overcome the bright sky background, the NIR offers several advantages over the optical when determining geometric properties of the stellar disk. It is significantly less sensitive to dust which will invariably attenuate and distort the flux (Driver et al. 2007) and in addition the NIR flux contribution of the young stellar population is only significant in moderately strong starbursts (Krueger, Fritze-v. Alvensleben & Loose 1995). Irregularities in morphology, such as randomly distributed H IIregions and associated Hα emission are therefore less significant, allowing a greater accuracy in determining the stellar galactic center (and the resulting ellipse) which might have otherwise been centered on an offset H_2 region.

When computing the parameters required for the KS relation, determinations of the disk radius employ the surface photometry from recent NIR Studies (Young et al. 2014; McCall et al. 2012; Kirby et al. 2008, Hereafter YJLK14, MVPB12, KRDJ08 respectively) which have precisely measured the stellar disks of various Local Volume galaxies, mostly consisting of dwarf irregulars, low-mass late types, and blue compact dwarf galaxies. Using NIR surface photometry is unusual in the sense that we could simply use the Holmberg diameters from de Vaucouleurs et al. (1991) and Lauberts & Valentijn (1989). It is expected that the 'equivalent' Holmberg radii in the NIR will still be more accurate, despite requiring the B-band magnitude to compute this parameter (see Section 2.2.3), for the reasons listed above.

In this study, the samples of YJLK14 and KRDJ08 are amalgamated to form the primary sample of galaxies since we have full access to their data and computed parameters. Together they form a sample of 79 galaxies with several properties. Firstly, a morphology which ranges from some low-mass ellipticals and high-mass lenticulars to many low-mass late types and dwarf irregulars. A broad range in stellar mass, $6.5 < \log_{10}(\mathcal{M}_*/\mathcal{M}_\odot) < 11$, with a sample median of 8.3. This sample is mostly dominated by low-mass late type galaxies and dwarf irregulars. Finally, the KJRD08 and YJLK14 samples conveniently trace the main cosmic structures of the Southern hemisphere out to 10 Mpc (the Sculptor and Cen A group, respectively).

To further supplement the YJLK14 and KRDJ08 samples, we also source data from the MVPB12 study. This is an amalgamated K_s-band data set of newly observed galaxies and previous photometric studies filtered to include only those galaxies for which a surface brightness profile was successfully fitted, and for which the tip of the red giant branch (TRGB) distance was reliably measured. In addition to their own observations, MVPB12 sourced galaxy photometry from Vaduvescu et al. (2005, 34 galaxies), Vaduvescu & McCall (2008, 17 galaxies) and Fingerhut et al. (2010, 80 galaxies). The MVPB12 sample contains a total of 66 star-forming dwarf irregulars, which we analyze in addition to the dwarf irregulars and low-mass late types found in the YJLK14, KRDJ08 samples for a total sample size of 145 Local Volume galaxies.

2.1.2 HI fluxes, gas densities

In ideal circumstances, suitably resolved H I data of dwarf irregulars would be used to measure the gas densities point by point, and compared to the associated SFR surface density such as has been conducted in the studies of Roychowdhury et al. (2015) and Bigiel et al. (2008). For dwarf galaxies, sensitivity and angular resolution of the H I maps can be a particularly constraining factor (although the availability of SFR tracers may be an equally constraining factor), and so other previous studies have measured surface densities averaged over the entire star-forming disk (Wyder et al. 2009; Roychowdhury et al. 2014). Most galaxies in the YJLK14, KRDJ08 and MVPB12 samples described above, do not have readily available resolved H I maps. In order to increase the statistics of dwarf galaxies in the make-up of the star formation relation diagram, we resort to deriving the atomic gas density from the available total H I fluxes, averaged within the geometric parameters derived from the NIR photometric samples.

We obtain H I fluxes, with a few exceptions, from the H I Parkes All Sky Survey (HIPASS) catalogues of Koribalski et al. (2004) (1000 Brightest Galaxy Catalog) and Meyer et al. (2004). The HIPASS sample was observed on the 64m Parkes radio telescope using the 21cm multi-beam reciever, a correlator bandwidth of 64 MHz divided into 1024 channels and beam-width of ∼15 arcmin (Staveley-Smith et al. 1996). The MVPB12 study has already compiled H I fluxes for their galaxies from other sources (see their Table 4) and we simply adopt their values for those galaxies. For other galaxies we have obtained H I data from either the Bouchard et al. (2005) or Begum et al. (2008, Faint Irregular Galaxies GMRT Survey - FIGGS) study.

It is possible that the derived gas surface densities would introduce a bias and slope offset in the data which will require correcting. Potential statistical biases resulting from this estimation is explored in Sect. 3.1.

2.1.3 UV and 24μm fluxes, SFR tracers

Studies comparing the SFR estimates derived from H α and UV fluxes for Local Volume galaxies have found fundamental discrepancies where in principle it is expected they should agree (Meurer et al. 2009; Lee et al. 2009; Karachentsev & Kaisina 2013). Hα flux is systematically lower relative to the Far-Ultraviolet (FUV) with decreasing luminosity, underestimating the flux relative to the FUV by up to an order of

magnitude. One explanation as Meurer et al. (2009) suggests, is that variations in the initial mass function (IMF) of low luminosity galaxies are responsible. This follows logically from the relative sensitivities of each tracer with respect to the IMF. Hα emission resulting from ionization of the surrounding ISM will require stars in excess of 15 $M_\odot$ whose ionizing flux is sufficiently strong. In contrast, ultraviolet emissions directly trace the photospheric emissions of stars of several solar masses (Kennicutt & Evans 2012). Other works by Fumagalli, da Silva & Krumholz (2011) and Weisz et al. (2012) instead suggest that temporal variation in the SFRs as the cause. The above mentioned stochastic effects pronounce the gap between the underlying and traced star formation rate, appear to affect Hα more significantly than FUV (da Silva, Fumagalli & Krumholz 2014; Roychowdhury et al. 2014). We therefore elect to use FUV fluxes when computing the SFR surface density.

As part of the 11Mpc Hα and Ultraviolet Galaxy (11HUGS) survey, Lee et al. (2011) presented UV photometry of a complete sample of Local Volume galaxies. We cross-correlate galaxies within the primary sample and MVPB12 extracting where available observed total FUV fluxes. In instances when a total FUV flux is not available, we instead use the aperture flux, defined as the aperture beyond which the flux error becomes 0.8 mag or where the intensity falls below the sky background level. Statistically, systematic differences between the aperture and total fluxes are negligible as shown in Fig. 1, especially when compared to other sources of systematic errors.

The major drawback of using the FUV flux is its sensitivity to dust absorption. A composite tracer (e.g. Hao et al. 2011) accounting for the stellar emission re-radiated in the infrared via dust will therefore provide a better estimate of the SFR, although it is expected that for our sample dominated by low metallicity dwarf galaxies, these corrections should be small. The Local Volume Legacy survey (Dale et al. 2009) is a legacy Spitzer Space Telescope volume limited survey designed to complement the 11HUGS and ACS Nearby Galaxy Survey Treasury (Dalcanton et al. 2009) with observations of the near, mid and infrared fluxes of nearby galaxies. Using the 24 micron fluxes, we are able to correct our SFR tracer dust extinction in ∼35% of our galaxies (for median change in the measured SFR of 0.04 dex).

2.2 Derived Parameters

In the following subsections we describe the methods used to obtain the SFR surface density and the atomic gas surface density. Table 1 compiles the sample observed properties while Table 2 lists the derived properties.

2.2.1 Estimating the SFR

For estimating the *FUV* traced SFR, we first correct the available asymptotic magnitude for Galactic extinction (Schlafly & Finkbeiner 2011) using the relation given by Karachentsev, Makarov & Kaisina (2013),

$$m_{0,FUV} = m_{FUV} - 1.93\,(A_B^G + A_B^i) \quad (1)$$

where A_B^G and A_B^i are the Galactic and internal extinction corrections respectively in the B-band. We make no attempts to correct for internal extinction at this stage, since we account for internal extinction later using the 24 micron flux. The FUV flux density (f_ν) is computed from the total FUV magnitude ($m_{FUV,0}$) given in Column 7 of Table 1,

$$f_\nu(\mathrm{erg\ s^{-1}\ cm^{-2}\ Hz^{-1}}) = 10^{-0.4\left(m_{FUV,0}+48.6\right)}. \quad (2)$$

Using the best available distances in the literature (Column 5 in Table 1) and the flux densities, we compute the FUV and 24 micron luminosities (L),

$$L = \nu f_\nu \times 4\pi D^2. \quad (3)$$

For a constant star formation rate over 100 Myr, solar metallicity and either a Salpeter (Salpeter 1955) or a Kroupa IMF (Kroupa 2001), the attenuation corrected FUV luminosity, $L(FUV)_{\rm corr}$ (Column 2 in Table 2), is given by Hao et al. (2011):

$$L(FUV,\mathrm{corr}) = L(FUV) + 3.89L(25\mu\mathrm{m}). \quad (4)$$

The Hao et al. (2011) recipe was derived using the Infrared Astronomical Satellite (*IRAS*) 25μm observations. We instead use the *Spitzer* 24μm flux (Column 8 in Table 1), which introduces an uncertainty of less than 0.3 mag (Hao et al. 2011) due to the systematically lower luminosities recovered by IRAS observations (Kennicutt et al. 2009, Fig. 1) relative to *Spitzer*. Galaxies in the YJLK14, MVPB12 and KRDJ08 samples without a 24μm flux have their values estimated using the following relationship as a zeroth order approximation.

$$\log_{10} L\,(24\mu\mathrm{m}) = 1.11^{+0.09}_{-0.09} \log_{10} \frac{\dot{M}_*}{[\mathrm{M}_\odot]} + 31.415^{+0.739}_{-0.739} \quad (5)$$

derived from the least squares regression of the galaxies with available 24μm flux measurements as shown in Fig. 2. As demonstrated, the 2σ trends provided reasonable upper and lower bound limits to the available data. We have conservatively elected to use the lower bound relationship to correct for dust since it is plausible that many dwarf galaxies in the

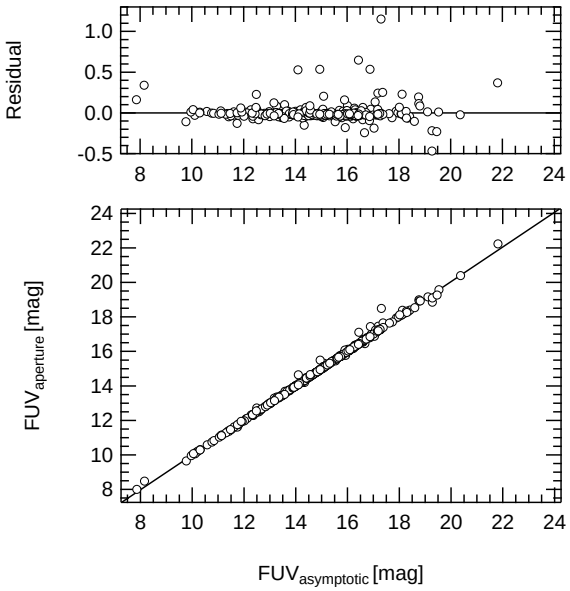


Figure 1. Comparing the aperture and asymptotically derived total FUV magnitudes from the 11HUGS survey.

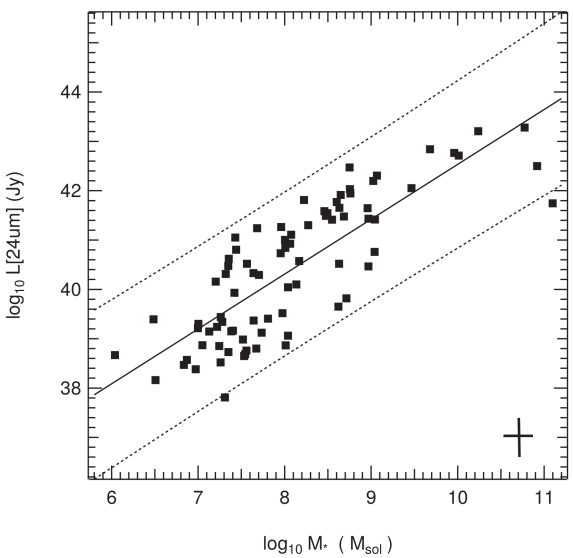


Figure 2. The relationship between the stellar mass and 24μm luminosity in YJLK14, MVPB12 and KRDJ08 sample galaxies. The solid line represents the least squares fit to the data. The dotted lines represent the upper and lower 2σ intervals. These intervals provide reasonable lower and upper bound estimates to the dust content as a function of stellar mass. The cross at the bottom-right shows representative 1σ errorbars.

sample have inconsequential dust content. We note that dust measurements remain a large source of uncertainty for those galaxies without a 24μm flux measurement, since the data are scattered over approximately 2 orders of magnitude.

Plugging the corrected FUV luminosity into the recipes prescribed by Kennicutt & Evans (2012) and Hao et al. (2011) we obtain the SFR ($\dot{M}_*$, Column 3, Table 2),

$$\log_{10} \frac{\dot{M}_*}{[\mathrm{M}_\odot\ \mathrm{yr}^{-1}]} = \log_{10} \frac{L(FUV, \mathrm{corr})}{[\mathrm{erg\ s}^{-1}]} - 43.35. \quad (6)$$

As to be expected for the dwarf and LSB galaxies, dust corrections to the SFRs are typically low. The median change in the measured SFR is 0.04 dex although a maximum of 0.5 dex is recorded indicating the importance of dust corrections in the case of some galaxies.

Star formation rate values from Wyder et al. (2009) and Kennicutt (1998) require a correction ($\dot{M}_* = 0.63\dot{M}_{*,K98}$) to account for updated stellar population models and the choice of IMF used in more modern studies. We have performed this correction in the analysis to bring them into line with more modern studies.

We calculate the uncertainty in the measurements by including the uncertainty in distance (typically between $\approx 10-20\%$), the flux and the errors in the calibration. To get total errors, we add these uncertainties in quadrature. In all the figures we show representative error bars, which were calculated as the average error on the quantities of the galaxies shown.

2.2.2 HI and gas mass estimation

We estimate the H I mass (compiled in Column 4, Table 2) for our sample galaxies following Roberts (1975),

$$M_{\mathrm{H\,I}} = 2.36 \times 10^5 D^2 F_{\mathrm{H\,I}}, \quad (7)$$

where D is the distance of the galaxy from the sun and $F_{\mathrm{H\,I}}$ is the 21 cm emission line flux (Column 9, Table 1). The dwarf and low-mass late type galaxies are assumed to have a negligible molecular fraction and so the total gas mass M_{gas} is simply the H I mass corrected for the presence of helium using a factor of 1.34.

2.2.3 Geometric and density computations

In order to find the NIR equivalent Holmberg radius $R_{26.5,eq}$, we use the extinction corrected $(B\text{-}H)_0$, and $(B\text{-}Ks)_0$ colours. YJLK14 demonstrated (their Figure 10) significant variation in the colours of dwarf galaxies and thus it is important to perform colour corrections directly rather than through the use of a scaling relationship.

The NIR equivalent Holmberg radius ($R_{26.5,eq}$) for the primary sample is computed from Equation 1 in YJLK14 and is given by

$$R_{26.5,eq} = [0.921(26.5 - [(B-H)_0]) - 0.921\mu_0]^{1/n}\ r_0, \quad (8)$$

where μ_0 is the central surface brightness in the H-band, n is the Sérsic index and r_0 is the scale length parameter in units of pc. Similarly, following from Equation 1 in MVPB12,

$$R_{26.5,eq} = \mathrm{acosh}\left[10^{[-0.4(\mu_0-(26.5-[(B-Ks)_0]))]}\right]\ r_0. \quad (9)$$

For the amalgamated MVPB12 sample, all parameters are generated using the semi-major axis as the native radial coordinate and so no further corrections are required to compute the area of the disk defined by the semi-major axis. The KRDJ08 and YJLK14 data was instead computed using the geometric mean radius. The area defined by the semi-major axial component of the $R_{26.5,eq}$ in this case is,

$$A = A_{26.5,eq} = \pi R^2_{26.5,eq}/(1-e), \quad (10)$$

where e is the measured ellipticity. The estimated SFRs and H I masses are averaged over this quantity to derive an estimate of the atomic gas and SFR surface densities for the NIR galaxy samples. Along with $R_{26.5,eq}$, the quantities are compiled in Table 2. The Tully & Fisher (1988) catalogue include an inclination corrected Holmberg diameter and it is therefore trivial to calculate the atomic gas and SFR surface densities.

3 RESULTS AND DISCUSSION

The main focus of the following discussions is to investigate the trends in the star formation relation in the H I dominated regime. Noting the limitations a linear model pose on an obviously multidimensional problem, a later section is dedicated to comparing the gathered data to various comprehensive models of star formation.

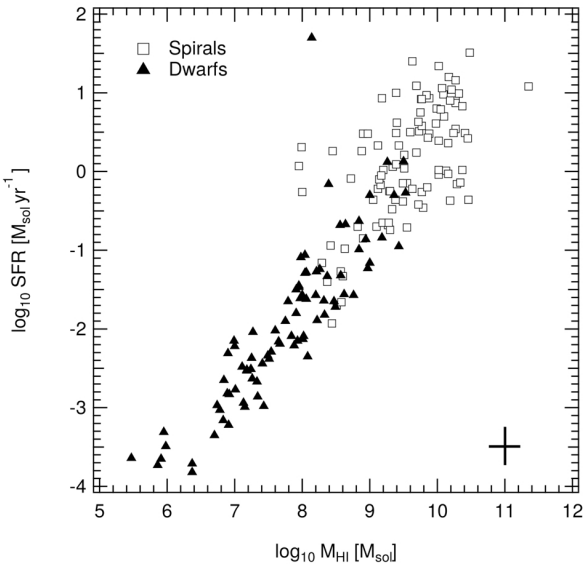


Figure 3. The relationship between the SFR and total H I mass in dwarf and spiral galaxies. Data for the dwarf galaxies were drawn from YJLK14 and KRDJ08. Data for the spiral galaxies were obtained from the NHICAT, HOPCAT and ALFALFA H I catalogues. Dwarf galaxies show a very consistent and linear relationship over a broad range of H I masses, but spiral galaxies display comparatively more scatter than dwarfs. The cross at the bottom-right shows representative 1σ errorbars.

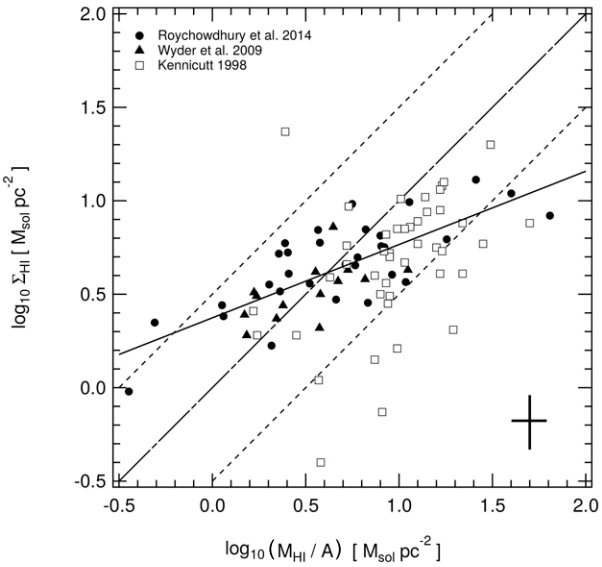


Figure 4. $\Sigma_{\rm H\,I}$ versus $M_{\rm H\,I}/A$ for the K98 spiral and Wyder et al. (2009) and Roychowdhury et al. (2014) dwarf sample galaxies. The broken solid line indicates a slope of unity. Dashed lines indicate offsets of 0.5 dex. The solid line shows the least squares regression to the low surface brightness galaxies from the Wyder et al. (2009) and Roychowdhury et al. (2014) samples (correlation coefficient 0.750). The cross at the bottom-right shows representative 1σ errorbars.

3.1 How accurate is $M_{\rm H\,I}/A$ as a proxy for $\Sigma_{\rm gas}$?

Before proceeding, we must ensure that $M_{\rm H\,I}/A$ is a valid proxy for $\Sigma_{\rm gas}$. The apparent correlation and linearity between the total atomic gas and the star formation rate as shown in Fig. 3 suggest this might be the case. Dwarf galaxies show a very consistent and linear relationship over a broad range of H I masses. The linearity of this relationship suggests that by normalizing to a fiducial disk area, such as that defined by the Holmberg diameter, we do not introduce a secondary effect on the measured slope of the linear regression to the data points. Of course, we may introduce a bias and an offset in the $\Sigma_{\rm gas}$ scale since by using the $M_{\rm H\,I}/A$ proxy we are insensitive to variation in the ratio of the optical-H I diameter (A is derived following the optical data).

In order to determine the typical value by which we over or under-estimate the actual gas surface density, we calculate $M_{\rm H\,I}/A$ for the spiral galaxies from K98, and the dwarf galaxies from Wyder et al. (2009) and Roychowdhury et al. (2014) comparing them to the $\Sigma_{\rm gas}$ calculated in the respective studies. As mentioned previously, we obtain global H I fluxes, inclinations and isophotal radii for the K98 galaxies from the Nearby Galaxy Atlas catalogue. For the low surface brightness galaxies, these quantities are obtained from the RC3 catalogue and for the Roychowdhury et al. (2014) these are obtained from Begum et al. (2008). Figure 4 plots the surface gas densities against the computed $M_{\rm H\,I}/A$ quantities. We emphasize A has been derived here not using the H I data but the optical data, i.e., considering the Holmberg radius and adding the factor $1/\cos i$ to include the geometric correction (see YJLS14). As shown in the plot, most data points are scattered around unity typically by within 0.5 dex. There is an obvious trend from overestimation to underestimation with increasing H I mass. Fortunately this bias appears to be linear and we correct for it using a least squares approach. The Pearson correlation coefficient of this fit is $r = 0.750$. We derive the correction

$$\log_{10}\Sigma_{\rm H\,I} = (0.4 \pm 0.1)\log_{10}(\rm M_{H\,I}/A_{26.5}) + (0.38 \pm 0.04), \quad (11)$$

(solid line in Fig. 4), which is applied before correcting for helium. We include the errors in the fit above when estimating the total errors in $\Sigma_{\rm HI}$ and $\Sigma_{\rm gas}$.

From Fig 4 and the demonstrated large scatter in the K98 sample, we recommend not to use this method in galaxies other than H I -dominated galaxies. Given that many dwarf galaxies, particularly those with distances larger than 11 Mpc, will remain unresolved for the foreseeable future – large H I surveys using the ASKAP and MeerKAT will typically have a beam size of ∼30", which is just 2–6 times smaller than the typical size of the H I distribution in dwarf galaxies of the Local Volume, (e.g. Koribalski et al. 2018), and hence only the closest dwarfs will be resolved in H I –, this method is the only way to compare dwarfs to spirals in statistically meaningful samples and it is therefore fortunate that the scatter for dwarf galaxies in Fig. 4 is within an order of magnitude and the bias is linear.

3.2 The Kennicutt-Schmidt relation for Local Volume galaxies

Using the data and derived parameters described in Section 2, we plot the gas and SFR surface densities. Figure 5 explores the simple linear regression to the SFR relation for low surface brightness galaxies from KRDJ08, YJLK14 and

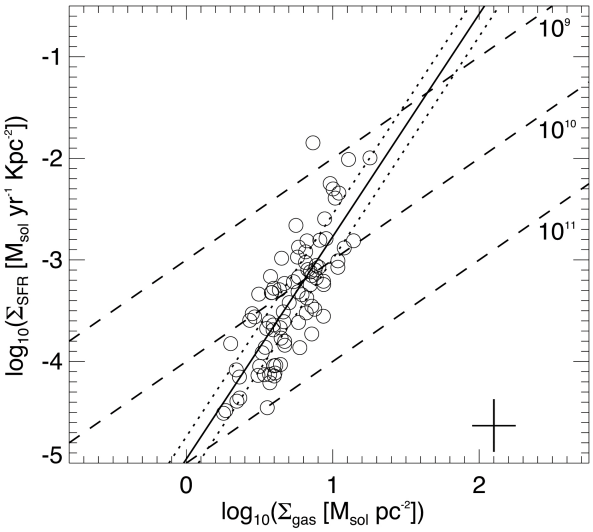


Figure 5. Surface density of the SFR as a function of the gas surface density for the low surface brightness galaxies obtained from the NIR samples, KRDJ08, YJLK14 and MVPB12 and whose atomic gas surface densities have been estimated from global parameters as outlined in Sect 2. Dashed lines corresponds to slopes of constant gas depletion times in units of years, as labelled. The solid black line corresponds to the best-fit obtained using `HYPER-FIT` (Robotham & Obreschkow 2015), adopting the conjugate gradients method. The dotted lines mark the 1σ uncertainty in the zero-point of the relation. The cross in the bottom-right of the panel shows a representative error bar of individual measurements.

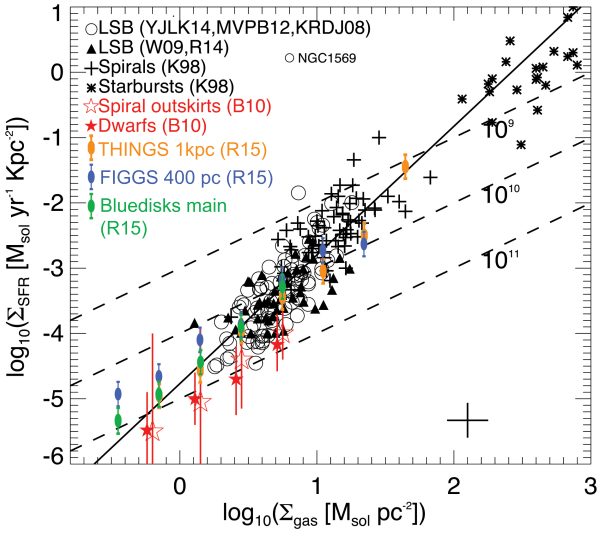


Figure 6. The Kennicutt-Schmidt relation for YJLK14, MVPB12 and KRDJ08 (*open circles*) sample galaxies compared to the original K98 data (*plus symbols* for spirals, *crosses* for starbursts). Additionally, we have included the disk averaged quantities for the galaxies whose column densities were measured directly (Roychowdhury et al. 2014; Wyder et al. 2009, *black triangles*). The open and filled stars with errorbars show the median and 1σ scatter of the spiral outskirts and dwarf galaxies of Bigiel et al. (2010), respectively, both of which correspond to H I -dominated regions. For clarity, we artificially displaced the medians of the dwarf galaxies by 0.04 dex in the x-axis. The Roychowdhury et al. (2015) data for their 'THINGS 1kpc' (orange circles), 'FIGGS 400pc' (blue circles) and 'Bluedisks main' (green circles) samples are also shown for comparison. The K98 galaxies have been corrected for the presence of helium contrary to the original work. The diagonal dashed lines corresponds to slopes of constant gas depletion times in units of years, as labelled. The solid line shows the best fit to selected data, as described in the text, using the same the procedure described in Fig. 5. The cross in the bottom-right of the panel shows a representative error bar of individual measurements.

MVPB12. Figure 6 extends the regression analysis to include low surface brightness galaxies and spiral galaxies from further sources (Roychowdhury et al. 2014; Wyder et al. 2009; Kennicutt 1998) whilst the outer disk (Bigiel et al. 2010; Roychowdhury et al. 2015) and starburst data (Kennicutt 1998) is included in the plot for comparative purposes only.

In order to obtain a best-fit to our data and quantify the power-law index of the relation $\Sigma_{\rm SFR} \propto \Sigma_{\rm gas}^{N}$, we use the `HYPER-FIT` R-package of Robotham & Obreschkow (2015). We perform the fits using the Optim algorithm with the conjugate gradients method, minimising the scatter orthogonal to the plane. In the fit we included the errorbars for individual objects, and assume that that the errors in the x and y axis are not correlated. The best fit obtained for the low surface brightness galaxies from KRDJ08, YJLK14 and MVPB12 is

$$\log_{10}\Sigma_{\rm SFR,LSB} = 2.19^{+0.25}_{-0.21}\log_{10}\Sigma_{\rm gas} - 4.96^{+0.22}_{-0.22} \qquad (12)$$

including all the data as outlined above, the corresponding best fitting relation is instead,

$$\log_{10}\Sigma_{\rm SFR,spirals\ and\ LSB} = 1.97^{+0.11}_{-0.1}\log_{10}\Sigma_{\rm HI+H_2} - 4.77^{+0.28}_{-0.28} \qquad (13)$$

Figure 5 shows that there is a clear correlation between the surface densities of the SFR and the atomic gas with a steep dependence on the latter quantity. Although we did not include the Bigiel et al. (2010) data in the least squares fit shown in Fig. 6, visual comparison of their data set to the line of best fit seems to show a good agreement, although we remind that the Bigiel et al. (2010) points have too high depletion time. We note, however, the narrow range in $\Sigma_{\rm HI}$ for our sample galaxies, which spans from 0.2 to 1.2 in log scale in Fig 4. This is a consequence of the fit to the data from Wyder et al. (2009) and Roychowdhury et al. (2014) samples that we apply to the unresolved HI data. Possible biases in the samples, for example by being sensitive to only a narrow range in $\Sigma_{\rm SFR}$ or $\Sigma_{\rm HI}$ (unlike the spiral galaxies from Kennicutt 1998, which span a much wider range in both axes), could lead to the data preferring an N=1 slope due to the reduced dynamic range. If this were the case, using resolved H I data to estimate H I distributions could change our results.

The slopes derived for the LSB galaxies in our study are much steeper than that found in Roychowdhury et al. (2014) and is more supportive of the findings of Roychowdhury et al. (2015). Roychowdhury et al. (2015) suggested this difference could be an effect of being biased towards the inner star-forming regions of galaxies. If that were the case, we might expect the same phenomenon in our sample galaxies which are also disk averaged quantities. Instead they form a tight distribution intermediate to the outer disk data of Bigiel et al. (2010) and the spirals of Kennicutt (1998). In-

deed, we note that the two determinations of the K-S relation slope (1.97 for the combined spirals+LSB sample and 2.19 for the LSB sample) agree within the fitting errors. Therefore, using the LSB sample we are probably circumventing any existing bias (as the mentioned narrow range in $\Sigma_{\rm H\,I}$) in the Wyder et al. (2009) and Roychowdhury et al. (2014) samples and reinforcing the results obtained by Kennicutt (1998).

Our sample includes galaxies over a much wider range of surface brightness than the sample of Roychowdhury et al. (2014): low surface brightness galaxies from YJLK14, the somewhat brighter low-mass late types and irregulars from KRDJ08, as well as star-forming dwarfs and additional low surface brightness galaxies from the amalgamated MVPB12 sample. We suggest that N=1 slope would be simply due to insufficient statistics especially given the generally good agreement between the Roychowdhury et al. (2014), Wyder et al. (2009) the novel KRDJ08, YJLK14 and MVPB12 datasets. For dwarf galaxies, we find a slope that is strictly not in agreement with the canonical N=1.4 derived from the original K98 sample. As Bigiel et al. (2008) noted, the N=1.4 relies on the contrast of spiral disks and the molecular rich circumnuclear starbursts.

Notably, the galaxy NGC 1569 (labelled in Fig. 6) lies well outside the expected behavior for spirals or dwarf galaxies. Environmental interactions resulting in the star-burst activity are very likely to be the cause of NGC 1569 significant offset from the star formation relation with respect to the broader population of galaxies (e.g. Mühle et al. 2005), as also discussed in the case of NGC 5253 (López-Sánchez 2010; López-Sánchez et al. 2012).

3.3 Comparing global and resolved properties

Above the critical density of the total gas ($\sim 9\ M_{\odot}{\rm pc}^{-2}$), in the H_2-dominated regions of their spiral galaxies, Bigiel et al. (2008) and Leroy et al. (2013b) found an universal molecular star formation relation with a corresponding exponent of N=1. Conversely, when looking at the corresponding total gas or H I gas star formation density diagrams, exponents are found to vary significantly radially within galaxies and from galaxy to galaxy. Above the critical density, the atomic gas saturates in these galaxies and there is no observed correlation between the atomic or total gas with the SFR. While, below the critical density where the gas is H I -dominated, the atomic gas and SFR surface densities correlate (Bolatto et al. 2011; Bigiel et al. 2010; Koribalski & López-Sánchez 2009; López-Sánchez et al. 2015). This relationship does not have a fixed slope.

Variation of the total gas SFR relations imply that the ratio of H I -to-H_2 can vary within galaxies and in between galaxies, or rather that the star formation efficiency (SFE) is not constant due to either local or global factors. More recent work has confirmed significant variation of the SFE between different THINGS galaxies (Shetty et al. 2014), but they studied the molecular hydrogen. While factors other than the surface density of the gas have been shown to influence the SFE, in their sample, Leroy et al. (2008) demonstrated where the ISM is dominated by atomic gas, such as in the outer disks of spirals, the SFE decreases with increasing radius, implicating a global radial dependence on SFE in addition to local variation. The studies of Roychowdhury et al. (2015) and Elmegreen & Hunter (2015) provide further evidence for radial dependance on the SFE.

Recently Wang et al. (2017) used high-quality interferometric H I data from the LVHIS (Local Volume H I Survey Koribalski et al. 2018), including a multi-wavelength dataset that allows to perform a careful estimation of the SFR, to find that the correlation between the globally averaged Σ_{SFR} and $\Sigma_{\rm H\,I}$ is weak. Their figure 11 shows these data; their galaxies seem to overlap on the scatter from our Fig. 6. They also found that the SFE significantly depends on the average stellar surface density, something that can be explained using a marginally stable disk model, as described in Wong et al. (2016). This was already explored by Shi et al. (2011), who proposed an explicit dependence of the SFE on the stellar mass surface density (the "extended Schmidt law"). The SFE-$\Sigma_{\rm star}$ relation proposed by Shi et al. (2011), that can be reproduced by some models and holds over five orders of magnitude in -$\Sigma_{\rm star}$ for individual global galaxies, included LSB and dwarf galaxies that deviate from the K-S law.

With the increase in sample size relative to prior studies, we are able to reproduce similar trends shown in resolved studies and reconcile some of the inconsistency introduced by Roychowdhury et al. (2014). Both resolved and disk averaged studies imply a 'floor' on the fraction of H_2 gas given the shape of the distributions in Fig. 6. The resolved and disk averaged data are not in complete agreement when it comes to the slope of the star formation relationship. Bigiel et al. (2010) and Roychowdhury et al. (2015) find exponents on average of N = 1.5 while this study finds a much steeper slope (N = 2.4) for the disk averaged data, albeit with a large uncertainty. This statistical uncertainty in the slope greatly decreases when including the spiral disk data from Kennicutt (1998) and this is reflected in the correlation coefficients of these fits increasing from r = 0.670 to 0.795.

Roychowdhury et al. (2015) suggested that this apparent inconsistency arises from the bias when looking at optical disk averaged quantities. It is possible to imagine resolved regions within a H I disk with similar gas surface densities to a disk averaged value for a given galaxy but with little or no star formation as they may lie outside the star forming disk. One potential means of resolving this inconsistency is to use the total area of the H I disk rather than the optical disk. This would require a trend in the optical to H I diameter such that galaxies with higher surface densities had a larger diameter ratio relative to galaxies with lower surface densities.

Ultimately as the distribution of points in Fig. 6 demonstrate, the star formation relationship is more complex than what linear relationships would imply. We note that our data occupy a narrow range of atomic surface densities, whilst the numerous resolved data points from Bigiel et al. (2010) occupy a much wider range and show a complex distribution. Within this distribution itself significant variation of the exponent of the star formation law is easily possible. We suggest that such variations in slope are an indicator of the complexity of the problem and that a more nuanced approach would be required to fully describe the distribution of the data. Section 4 describes the available comprehensive models dealing with the star formation relationship and compares the available data to them in order to obtain greater insight.

3.4 Physical causes for the variation in the SFE

At least some of the scatter, and therefore the overall offsets in the distribution of the Local Volume galaxies, particularly the dwarfs, must occur from variations in the scale height of the disk. Schmidt (1959) originally proposed that $\rho_{SFR} \sim (\rho_{\rm gas})^n$, whereby $\rho_{\rm SFR}$ and $\rho_{\rm gas}$ are the SFR and gas volume densities respectively. For constant scale-heights, such as in ideal spirals whose intrinsic axial ratio is well known ($\sim$ 0.2), projection effects play no part in the variation of SFE. There is evidence that Local Volume galaxies and dwarfs do not have a constant scale-height (Roychowdhury et al. 2010, 2013).

Modeling a galaxy's stellar discs as triaxal ellipsoids, Roychowdhury et al. (2013) used Monte Carlo simulations to determine the minor (q) and major (p) intrinsic axial ratios of irregular galaxies of the Local Volume. These galaxies demonstrated a significant degree of variation in their intrinsic axial ratios $0 < q_0 < 1$, which was mildly correlated with luminosity. Perhaps of more relevance to this study is the intrinsic axial ratio of the gas distribution. For a sample of faint dwarf irregulars from the FIGGS sample, Roychowdhury et al. (2010) determined a mean axial ratio of $\langle q \rangle \sim 0.6$ for their sample. Note, however, that the axial ratio of $\langle q \rangle$ provided by Roychowdhury et al. (2010) had a large associated error, and therefore a large intrinsic variation in the ratio from galaxy to galaxy is expected.

Assuming a disk in which the gas volume density decays exponentially, the surface density $\Sigma_{\rm gas}$ and central volume density $\rho_{0,\rm gas}$ is related by the scale height as $\rho_{0,\rm gas} = \Sigma_{\rm gas}/(2h)$. As in the LSB galaxies in the Wyder et al. (2009) and the Roychowdhury et al. (2014) sample, the Local Volume galaxies in this study also display a factor $\sim$5 offset in gas depletion times to the spiral in the original K98 sample, which if entirely attributable to changes in scale height, would imply that late type and irregular galaxies have discs with significantly larger scale heights relative to spiral galaxies.

Relatively speaking, potentially thicker disk scale-heights in dwarf irregulars would lead to a lower effective volume density, increased free fall time and thus lower observed SFE. Indeed in their study of 20 dwarf irregular galaxies, Elmegreen & Hunter (2015) considered the effects of disk thickness extensively. The dwarf galaxies in their sample were shown to be thick in absolute terms, with gas scale heights of 0.5 kpc and a typical ratio of scale height to radius of 0.6. Remarkably, correcting for the free fall time of the atomic gas (see Eq. 14) yields an efficiency $\epsilon_{\rm ff}$ of one per cent, which is the also the SFE of the molecular gas. In other words the atomic gas is consumed at the same rate as molecular suggesting their ratios are fixed.

Dwarf galaxies are H I -dominated and so the molecular fraction is expected to be low which also simultaneously leads to a lower effective SFE of the total gas. Measuring the molecular fraction in low metallicity galaxies is challenging, due to the very high ratio of CO-to-H_2 column densities (Bolatto, Wolfire & Leroy 2013), although CO observations (e.g. Schruba et al. 2012) and dust emission studies (Bolatto et al. 2011) suggest that the molecular gas fraction should be very low. For example, Bolatto et al. (2011) derives a molecular fraction of only 5% for the Small Magellanic Cloud (SMC) using high-resolution H I and dust emission maps.

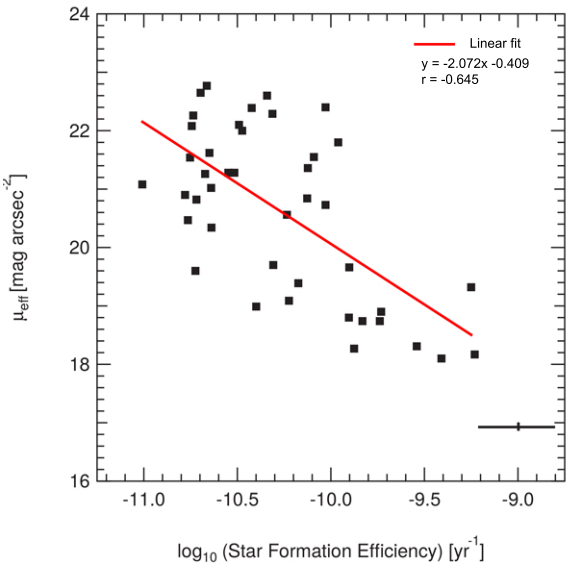


Figure 7. Comparing the estimated star formation efficiency against the NIR mean surface brightness, for galaxies in the YJLK14 and KRDJ08 samples. The cross at the bottom-right shows representative 1σ errorbars. The red continuous line is a linear fit to the data.

Given that the SFE of the atomic gas and molecular gas are found to be similar, it should be possible to estimate the fraction of molecular gas by comparing the atomic and molecular star formation laws and having adjusted for free fall times (or in our case a disk thickness factor.

Although evidence in general supports dwarf irregulars having thick disks (e.g. Roychowdhury et al. 2010; Elmegreen & Hunter 2015), direct measurement of the three dimensional shape of the dwarf galaxies DDO 46 and DDO 168 using the central stellar dispersion to the ratio of the maximum rotation speed by Johnson et al. (2015), suggest that these galaxies are comprised of thin stellar disk. If gas disks in dwarf galaxies were also thin, the estimation of the molecular fraction in these systems should also account for the possibility of varying disk thickness and free fall times.

To attempt an estimation of the typical molecular fraction we consider only variations in disk scale height and molecular fractions. We ignore other factors which might affect the SFE. First we assume that disk scale heights are largely consistent within the dwarf galaxy sample and following from Roychowdhury et al. (2010) the disk thickness is statistically $\sim$2.5 times thicker than the typical spiral. Using the relationship between molecular gas and SFR surface densities from Leroy et al. (2013b), our galaxies are offset by a factor of approximately 15-20 to the expected value. However since the disk is potentially 2.5 times effectively less dense than for those in spirals due to an increased scale height this factor is perhaps closer to 6-8 times corresponding to a typical molecular fraction of $\sim$ 0.16, or in the case of a thin disk 0.05.

In their analysis of a sample of low surface brightness (LSB) galaxies Wyder et al. (2009) suggested that a relative decrease in the molecular fraction in environments below the saturation limit, $\Sigma_{\rm H\,I} \approx 9$ M$_\odot$ pc^{-2} as a possible expla-

nation for the decreased SFE. Following the suggestions of Blitz & Rosolowsky (2006), that the ratio of molecular-to-atomic gas in galaxies is determined by hydrostatic pressure in the ISM, which is a function of the stellar surface density, the gas surface density, and the gas-to-stellar velocity dispersion ratio, Wyder et al. (2009) argues that the LSB galaxies will invariably have a lower ISM pressure and thus lower molecular fraction.

We explore this possibility by examining the H-band mean effective surface brightness against the star formation efficiency for the KRDJ08 and YJLK14 samples in Fig. 7. As discussed in KRDJ08 and YJLK14, we can use the H-band surface brightness as a proxy for stellar surface density, $\Sigma_{\rm star}$. The data in Fig. 7 covers six orders of magnitude in surface brightness and is well scattered with a minor trend towards higher SFE with higher surface brightness. A linear fit to the data (red continuous line in Fig. 7) provides a correlation coefficient of $r = -0.645$. This suggests that the stellar densities play a minor role in setting the SFE amongst the various dwarf galaxies. Many of the galaxies in Fig. 7 approach surface brightnesses typical of late type spirals found in the 2MASS Large Galaxy Atlas (Jarrett et al. 2003) yet have a much larger range of SFEs. In relative terms, it would appear that the lower stellar densities relative to the spiral population play a minor role in setting the SFE.

However, we note that, following Shi et al. (2011) and Wang et al. (2017), an effect of the $\Sigma_{\rm star}$ should be expected, as introduced in the extended Schmidt law. Recently Roychowdhury, Chengalur & Shi (2017) used data from the FIGGS survey to show that low-metallicity faint dwarf galaxies also followed the extended Schmidt law. They found that the mean deviation of the FIGGS galaxies from the extended Schmidt law is 0.01 dex, with a scatter around the relation of less than half that seen in the original Shi et al. (2011) relation. A precise determination of the SFE (i.e, performing a detailed SFR study and deriving the amount of neutral gas using interferometric maps) should be obtained to explore further this issue using our galaxy sample

4 COMPARISONS TO MODELS

In the previous sections, we attempted to describe the vertical offset displayed by the dwarf galaxies in Fig. 6 in terms of variations in their disk or molecular fraction. Krumholz, Dekel & McKee (2012) demonstrated that in the case of the molecular star formation relation, much of the observed scatter could be reduced by normalizing the molecular gas mass per free fall time,

$$\Sigma_{\rm SFR} = f_{H_2} \epsilon_{\rm ff} \frac{\Sigma_{\rm gas}}{t_{\rm ff}} \tag{14}$$

$$t_{\rm ff} = \sqrt{\frac{3\pi}{32 G \rho}} \tag{15}$$

where ρ is the density of the star-forming complex, f_{H_2} is the fraction of the molecular gas and $\epsilon_{\rm ff}$ is a dimensionless SFE scale factor. Since in extra-galactic observations of regular spirals the resolution does not approach that of a giant molecular cloud, the mean surface gas densities are instead representative of the ISM. In the case where star formation occurs in a galaxy primarily through GMC complexes, Krumholz, Dekel & McKee (2012) show that the free fall time can be estimated from easily observed projected quantities,

$$t_{\rm ff} = \frac{\pi^{1/4}}{\sqrt{8}} \frac{\sigma}{G \left(\Sigma_{\rm GMC}^3 \Sigma_{\rm gal}\right)^{1/4}} \tag{16}$$

where $\Sigma_{\rm GMC}$ is the mean gas surface density of GMCs value adopted from local observations, σ is the local velocity dispersion of the gas and $\Sigma_{\rm gal}$ is the average gas surface density in the region of the galaxy where the GMCs form. Since variations in disk scale height should result in relative changes of the volume density of the gas and therefore the free fall time, for a given mean value of the gas velocity dispersion within the star-forming disk, the free fall time could be estimated. Applying Equation 14, having now accounted for projection effects, any remaining vertical offset between dwarf and spiral galaxies could be more precisely attributed to variations in f_{H_2}, the molecular fraction of the gas.

As demonstrated by Leroy et al. (2013b) and Shetty et al. (2014), any star formation relation is ultimately a multidimensional problem and potentially even a multivalued function of $\Sigma_{\rm gas}$. Using observations to constrain the inputs, comparisons to models with varying underlying theoretical assumptions could provide greater insight into the processes which regulate star formation. Indeed, the correlation between atomic gas and the SFR surface densities in H I -dominated regimes, as demonstrated in this study and others (Bigiel et al. 2010; Bolatto et al. 2011; Roychowdhury et al. 2014, 2015), has been the subject of interest in recent models (Ostriker, McKee & Leroy 2010; Krumholz 2013), whose underlying theoretical assumptions differ.

In the Ostriker, McKee & Leroy (2010) model (hereafter OML), the ISM is comprised of warm and cold diffuse gas and a gravitationally bound phase. Star formation occurs in the gravitionally bound component without explicit treatment of its chemical state, at a rate corresponding to a fiducial choice in gas depletion timescale of 2 Gyr. The ISM satisfies thermal and vertical hydrostatic equilibrium whereby the UV heating (proportional to the star formation rate) can be balanced against the midplane density. The transition from H I -to H_2-dominated gas, and the effect gas metallicity has on it in the OML10 model, is not treated explicitly but manifests itself instead where the composition of the ISM transitions from mostly diffuse to mostly gravitationally bound. This transition happens smoothly, and will be an important factor when comparing models later. Alternatively, the Krumholz (2013, hereafter, KMT+) model, a low surface density extension to (Krumholz, Dekel & McKee 2012, hereafter KMT), explicitly determines the fraction of gas in the molecular phase which corresponds to the gas phase that is eligible to form stars. The fraction of the gas that is H_2 is calculated from the gas metallicity through dust shielding and through the photo-dissociation rate, as described in (Krumholz, McKee & Tumlinson 2008, 2009a). Perhaps motivated by a desire to reproduce recent resolved observations of H I -dominated galaxies (Bigiel et al. 2010) and the SMC (Bolatto et al. 2011), Krumholz (2013) successfully developed a model which predicts a floor in the star formation rate surface density. They argue that the interstellar radiation field (ISRF) intensity is not sufficient enough to satisfy hydrostatic equilibrium in the ISM of H I -dominated galaxies. By considering hydrostatic balance alone, a 'floor'

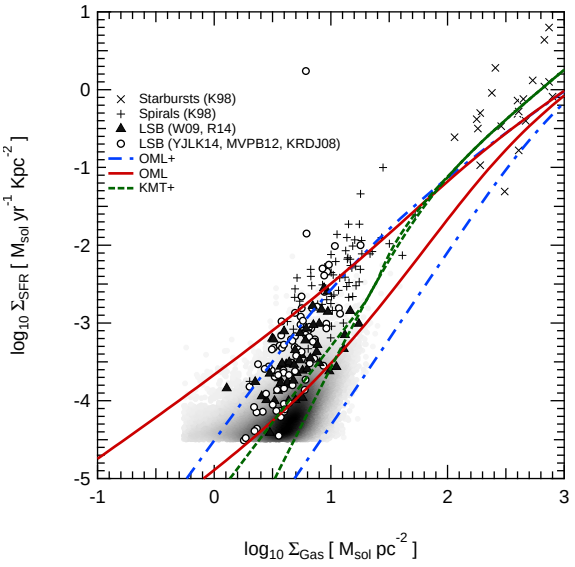


Figure 8. The log star formation rate versus total gas surface densities. Dwarf galaxies are assumed to have a negligible molecular fraction and so their total gas surface density is simply the atomic gas corrected for the presence of helium using a factor of 1.34. The K98 galaxies have been corrected for the presence of helium contrary to the original work. Filled triangles indicate disk averaged quantities for the galaxies whose column densities were measured directly from the Roychowdhury et al. (2014); Wyder et al. (2009) studies. Open circles indicate galaxies whose total gas surface densities have been estimated using global H I properties as described in the text. The greyscale smoothed distribution represents the outer disk data of H I -dominated dwarf and spirals galaxies from Bigiel et al. (2010) (shown in Fig. 6 as stars with errorbars). The models are indicated by the lines in the legend and are described in detail in the text.

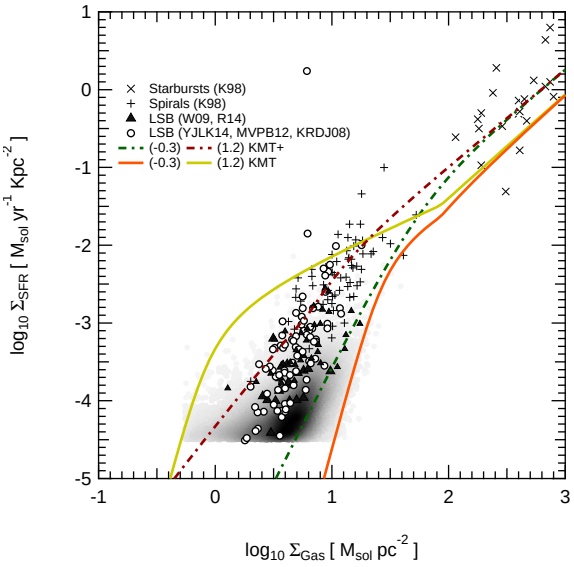


Figure 9. As in Fig. 8 but exclusively for the KMT and KMT+ models over a range of clumping factors, $-0.3 < \log_{10}(f_c Z_*) < 1.2$. The agreement between the KMT model and the data is good but requires an unreasonably large variation in clumping factors (see text for further details).

value on the density of the cold atomic phase can be determined, which can then be equated to a molecular fraction and star formation rate.

Figure 8 compares the KMT+, OML and the Bolatto et al. (2011, hereafter, OML+) (modification of the original OML by introducing an extra metallicity dependence). These models have been computed with the following parameters. Based on the discussions of Ostriker, McKee & Leroy (2010), and Krumholz (2013) we adopted a ratio of the mass-weighted mean thermal velocity dispersion, where if significant warm neutral medium is present, is approximately equal to the fraction of diffuse warm gas, $\tilde{f_w} \approx f_w = 0.5$. Variations in this quantity are degenerate with the midplane density parameter, $\rho_{\rm sd}$, for which we have adopted values in the range of 0.3-0.003 $M_\odot$ pc^{-3} in line with the ranges in other studies (e.g. Roychowdhury et al. 2015, 2014; Krumholz 2013). For the OML and OML+ models, values of the observed total velocity dispersion divided by the mean thermal value are ranged from two to 10 as per their discussions to produce the widest range in model tracks. For the KMT+ model, a clumping factor of $f_c = 5$ is adopted, which is the expected reduction factor in the mean surface density of cloud complexes when averaged over the ISM on kpc scales. All models are computed with a stellar metallicity of Z = 0.1 Z$_\odot$.

Figure 8 illustrates the success with which these models describe various datasets. The H I -dominated outer disk data from Bigiel et al. (2010) is well described by the OML+ and KMT+ models. However, Roychowdhury et al. (2015) observations matched better with the predictions of the OML model than those provided by the KMT model for galaxies of all types. The physical implications of the introduced metallicity dependence are unclear for the OML+ model (see section 4.3 of Krumholz 2013). In the KMT+ model, this metallicity dependent transition arises naturally from self-shielding of the molecular gas, however since the contrast between the self-shielded H_2 and transparent gas is very sharp, the KMT tracks converge faster than the OML and OML+ models (in these models the metallicity is degenerate with the midplane density parameter). The KMT+ model appears to be the most successful model when providing a 'floor' on the SFE and describing the transition from H I -dominated to H_2-dominated gas.

Over the range of adopted fiducial parameters however, the KMT+ model can not adequately describe the disk-averaged dwarf and low-mass late type galaxy measurements as shown in Fig. 8 as open circles and filled triangles respectively. We consider that this is unlikely the result of a metallicity effect. Following the stellar mass-metallicity relation presented by Kirby et al. (2013), galaxies with stellar masses less than 10^9 $M_\odot$are not expected to have stellar metallicities higher than Z = 0.1 Z$_\odot$ (see their Fig. 9). We clarify we are referring to stellar metallicities, galaxies with stellar masses less than 10^9 $M_\odot$will typically have gas-phase metallicities in the range of Z = 0.08 – 0.3 Z$_\odot$ (e.g. López-Sánchez 2010). The OML and OML+ models are not particularly sensitive to metallicity over the range of $0.01 < Z_* < 0.1$, and these variations are degenerate with stellar density. Similarly in the KMT+ model, metallicity variations do not change the overall picture, rather metallicity determines the location of the transition from H I -to-H_2 dominated gas.

The implication is that in the outer disks of spirals and dwarf galaxies, hydrostatic balance alone is sufficient to describe the star formation rates, but mean values of the overall disks of these low-mass galaxies suggest that thermal pressure provides an important contribution and is required to explain the full range of the data. This is consistent with the conclusions of Elmegreen & Hunter (2015), who found that models considering thresholds in the presence of H_2 did not agree with the smooth trends observed for the disks of the dIrr sample.

It is worth noting that 2 orders of magnitude in midplane density is quite generous, and although in general we do not have a handle on this quantity, 0.3 $M_\odot$ pc^{-3} is already a factor of ten times larger than values that have been inferred in galaxies (e.g. Bruzzese et al. 2015). Restricting this value further suggests that the OML model under-predicts the observed star formation rate densities. Alternatively, the original KMT model (Krumholz, McKee & Tumlinson 2009b) can describe the full range of the data if one relaxes the restriction on the clumping factor f_c. Figure 9 compares the KMT and KMT+ models with a range of $-0.3 < \log_{10}(f_c Z_*) < 1.2$, and in the case of the KMT+ model, a range of midplane densities an order of magnitude smaller than in Fig. 8 (0.03-0.003 $M_\odot$ pc^{-3}) was adopted. The original KMT model adequately describes the full range of the data with these model parameters. However while perhaps appropriate when describing variation in spiral galaxies, a $\log_{10}(f_c Z_*)$ value of 1.2 for a metallicity $Z_* = 0.1$ in units of solar metallicity suggests clumping factors an order of magnitude higher than that fiducial value of five adopted here and in tension with observations (Leroy et al. 2013a).

Variations in the underlying IMF and non-constant SFHs leading to systematic variations in the SFR estimates may explain this discrepancy. Although a full treatment of this topic is outside the scope of this work, we redirect the reader to Boquien, Buat & Perret (2014), Weisz et al. (2012) and Fumagalli, da Silva & Krumholz (2011). Recent observations with the STARBIRDS sample of galaxies by McQuinn et al. (2015) suggest an empirical calibration of the FUV-based SFR relation for dwarf galaxies, which is ∼53% more than Hao et al. (2011) which would increase the SFRs by a factor of 1.5 and further worsens agreement between the models and data presented here.

5 SUMMARY

We have provided a method for estimating the surface density of the atomic gas from global H I parameters which are widely available from H I surveys, and precision geometric parameters available from stellar photometry. We test this method using two control samples and find the approximation overestimates the actual surface gas density in H I -dominated galaxies to within a factor of 0.5 dex. We apply this method to a sample of 147 galaxies drawn from modern NIR stellar photometric surveys cross correlated with available *FUV* and 24μm fluxes to estimate the star formation rate surface density.

With this sample we confirm a strict correlation between the H I surface gas density and the SFR surface density with a sample of dwarf galaxies an order of magnitude larger than previous works. We find that the SFE of H I -dominated gas is offset from that in spirals. With considerations for variations of disk scale heights, we infer from relative comparison to molecular star formation relations that the mean molecular fractions in low-mass late types fall within 5-15%. Our analysis suggests that the stellar densities play a minor role in setting the SFE amongst the various dwarf galaxies, although following recent work we consider that using accurate, interferometric H I data we might recover the proposed extended Schmidt law which relates $\Sigma_{\rm SFR}$, $\Sigma_{\rm gas}$ and $\Sigma_{\rm star}$.

Finally we have compared our data and others from the literature to available models. We show that no single model can describe the full extent of the data. However these models together suggest that feedback is of variable importance depending on the density regime or galaxy environment, and that the transition from H I to H_2-dominated is a metallicity dependent process. Mean values of $\Sigma_{\rm SFR}$ and $\Sigma_{\rm gas}$ suggest that globally in these H I -dominated galaxies, thermal pressure is an important regulatory process.

ACKNOWLEDGMENTS

CL is funded by a Discovery Early Career Researcher Award (DE150100618). TY would like to thank the Research School of Astronomy and Astrophysics, CSIRO Astronomy and Space Science division and the Australian Astronomical Observatory through their support with the Research Training Scheme, ATNF Graduate program and the Trevor Burgess Scholarship respectively. HJ acknowledges the support of the Australian Research Council through Discovery Projects DP120100475 and DP 150100862. The Authors would like to extend their gratitude to Roychowdhury et al. (2014) for kindly providing a copy of their data. The authors also thank the anonymous referee for their very constructive comments that have helped to improve the quality of this paper. Parts of this research were conducted by the Australian Research Council Centre of Excellence for All-sky Astrophysics (CAASTRO), through project number CE110001020. Parts of this research were supported by the Australian Research Council Centre of Excellence for All Sky Astrophysics in 3 Dimensions (ASTRO 3D), through project number CE170100013.

APPENDIX

We include here the table listing the externally obtained properties required to compute the surface densities for the KRDJ08 and YJLK14 NIR samples (Table 1) and the table listing the computed quantities for the NIR catalogue galaxies (Table 2).

REFERENCES

Barazza F. D., Binggeli B., Prugniel P., 2001, A&A, 373, 12
Begum A., Chengalur J. N., Karachentsev I. D., Sharina M. E., Kaisin S. S., 2008, MNRAS, 386, 1667
Bigiel F., Leroy A., Walter F., Blitz L., Brinks E., de Blok W. J. G., Madore B., 2010, AJ, 140, 1194
Bigiel F., Leroy A., Walter F., Brinks E., de Blok W. J. G., Madore B., Thornley M. D., 2008, AJ, 136, 2846

Blitz L., Rosolowsky E., 2006, ApJ, 650, 933
Bolatto A. D. et al., 2011, ApJ, 741, 12
Bolatto A. D., Wolfire M., Leroy A. K., 2013, ARA&A, 51, 207
Boquien M., Buat V., Perret V., 2014, A&A, 571, A72
Bouchard A., Jerjen H., Da Costa G. S., Ott J., 2005, AJ, 130, 2058
Bremnes T., Binggeli B., Prugniel P., 1998, A&AS, 129, 313
Bremnes T., Binggeli B., Prugniel P., 1999, A&AS, 137, 337
Bremnes T., Binggeli B., Prugniel P., 2000, A&AS, 141, 211
Bruzzese S. M., Meurer G. R., Lagos C. D. P., Elson E. C., Werk J. K., Blakeslee J. P., Ford H., 2015, MNRAS, 447, 618
Cannon J. M., Dohm-Palmer R. C., Skillman E. D., Bomans D. J., Côté S., Miller B. W., 2003, AJ, 126, 2806
da Silva R. L., Fumagalli M., Krumholz M. R., 2014, MNRAS, 444, 3275
Dalcanton J. J. et al., 2009, ApJS, 183, 67
Dale D. A. et al., 2009, ApJ, 703, 517
de Swardt B., Kraan-Korteweg R. C., Jerjen H., 2010, MNRAS, 407, 955
de Vaucouleurs G., de Vaucouleurs A., Corwin, Jr. H. G., Buta R. J., Paturel G., Fouqué P., 1991, Third Reference Catalogue of Bright Galaxies. Volume I: Explanations and references. Volume II: Data for galaxies between 0^h and 12^h. Volume III: Data for galaxies between 12^h and 24^h.
de Vaucouleurs G., de Vaucouleurs A., Corwin J. R., 1976, in Second reference catalogue of bright galaxies, 1976, Austin: University of Texas Press., p. 0
Doyle M. T. et al., 2005, MNRAS, 361, 34
Driver S. P., Popescu C. C., Tuffs R. J., Liske J., Graham A. W., Allen P. D., de Propris R., 2007, MNRAS, 379, 1022
Elmegreen B. G., Hunter D. A., 2015, ApJ, 805, 145
Fingerhut R. L. et al., 2010, ApJ, 716, 792
Fu J., Guo Q., Kauffmann G., Krumholz M. R., 2010, MNRAS, 409, 515
Fumagalli M., da Silva R. L., Krumholz M. R., 2011, ApJ, 741, L26
Furlong M. et al., 2015, MNRAS, 450, 4486
Grisé F., Pakull M. W., Soria R., Motch C., Smith I. A., Ryder S. D., Böttcher M., 2008, A&A, 486, 151
Hao C.-N., Kennicutt R. C., Johnson B. D., Calzetti D., Dale D. A., Moustakas J., 2011, ApJ, 741, 124
Holmberg E., 1958, Meddelanden fran Lunds Astronomiska Observatorium Serie II, 136, 1
Hunter D. A. et al., 2012, AJ, 144, 134
Jarrett T. H., Chester T., Cutri R., Schneider S. E., Huchra J. P., 2003, AJ, 125, 525
Jerjen H., Binggeli B., Freeman K. C., 2000, AJ, 119, 593
Jerjen H., Freeman K. C., Binggeli B., 2000, AJ, 119, 166
Johnson M. C., Hunter D., Wood S., Oh S.-H., Zhang H.-X., Herrmann K. A., Levine S. E., 2015, AJ, 149, 196
Karachentsev I. D. et al., 2006, AJ, 131, 1361
Karachentsev I. D. et al., 2003a, A&A, 404, 93
Karachentsev I. D., Kaisina E. I., 2013, AJ, 146, 46
Karachentsev I. D., Karachentseva V. E., Huchtmeier W. K., Makarov D. I., 2004, AJ, 127, 2031
Karachentsev I. D., Makarov D. I., Kaisina E. I., 2013, AJ, 145, 101
Karachentsev I. D. et al., 2003b, A&A, 398, 479
Karachentsev I. D. et al., 2002a, A&A, 385, 21
Karachentsev I. D. et al., 2000, ApJ, 542, 128
Karachentsev I. D. et al., 2002b, A&A, 389, 812
Karachentsev I. D. et al., 2007, AJ, 133, 504
Kennicutt R. C., Evans N. J., 2012, ARA&A, 50, 531
Kennicutt, Jr. R. C., 1998, ARA&A, 36, 189
Kennicutt, Jr. R. C. et al., 2007, ApJ, 671, 333
Kennicutt, Jr. R. C. et al., 2009, ApJ, 703, 1672
Kirby E. M., Jerjen H., Ryder S. D., Driver S. P., 2008, AJ, 136, 1866
Kirby E. N., Cohen J. G., Guhathakurta P., Cheng L., Bullock J. S., Gallazzi A., 2013, ApJ, 779, 102
Koribalski B. S., 2008, The Local Volume HI Survey (LVHIS), Koribalski B. S., Jerjen H., eds., p. 41
Koribalski B. S., 2012, PASA, 29, 359
Koribalski B. S., López-Sánchez Á. R., 2009, MNRAS, 400, 1749
Koribalski B. S. et al., 2004, AJ, 128, 16
Koribalski B. S. et al., 2018, MNRAS
Kouwenhoven M. B. N., Bureau M., Kim S., de Zeeuw P. T., 2007, A&A, 470, 123
Kroupa P., 2001, MNRAS, 322, 231
Krueger H., Fritze-v. Alvensleben U., Loose H.-H., 1995, A&A, 303, 41
Krumholz M. R., 2013, MNRAS, 436, 2747
Krumholz M. R., 2014, Phys. Rep., 539, 49
Krumholz M. R., Dekel A., McKee C. F., 2012, ApJ, 745, 69
Krumholz M. R., McKee C. F., Tumlinson J., 2008, ApJ, 689, 865
Krumholz M. R., McKee C. F., Tumlinson J., 2009a, ApJ, 693, 216
Krumholz M. R., McKee C. F., Tumlinson J., 2009b, ApJ, 699, 850
Kuhlen M., Krumholz M. R., Madau P., Smith B. D., Wise J., 2012, ApJ, 749, 36
Lagos C. D. P., Lacey C. G., Baugh C. M., Bower R. G., Benson A. J., 2011, MNRAS, 416, 1566
Lauberts A., Valentijn E. A., 1989, The surface photometry catalogue of the ESO-Uppsala galaxies
Lee J. C. et al., 2011, ApJS, 192, 6
Lee J. C. et al., 2009, ApJ, 706, 599
Leroy A. K. et al., 2013a, ApJ, 769, L12
Leroy A. K., Walter F., Brinks E., Bigiel F., de Blok W. J. G., Madore B., Thornley M. D., 2008, AJ, 136, 2782
Leroy A. K. et al., 2013b, AJ, 146, 19
López-Sánchez Á. R., 2010, A&A, 521, A63
López-Sánchez Á. R., Koribalski B. S., van Eymeren J., Esteban C., Kirby E., Jerjen H., Lonsdale N., 2012, MNRAS, 419, 1051
López-Sánchez Á. R., Westmeier T., Esteban C., Koribalski B. S., 2015, Monthly Notices of the Royal Astronomical Society, 450, 3381
Makarova L. N., Karachentsev I. D., Grebel E. K., Harbeck D., Korotkova G. G., Geisler D., 2005, A&A, 433, 751
McCall M. L., Vaduvescu O., Pozo Nunez F., Barr Dominguez A., Fingerhut R., Unda-Sanzana E., Li B., Albrecht M., 2012, A&A, 540, A49
McQuinn K. B. W., Skillman E. D., Dolphin A. E., Mitchell N. P., 2015, ApJ, 808, 109
Metcalfe N., Godwin J. G., Peach J. V., 1994, MNRAS, 267, 431
Meurer G. R. et al., 2009, ApJ, 695, 765
Meyer M. J. et al., 2004, MNRAS, 350, 1195
Mühle S., Klein U., Wilcots E. M., Hüttemeister S., 2005, AJ, 130, 524
Noeske K. G., Papaderos P., Cairós L. M., Fricke K. J., 2003, A&A, 410, 481
Ostriker E. C., McKee C. F., Leroy A. K., 2010, ApJ, 721, 975
Parodi B. R., Barazza F. D., Binggeli B., 2002, A&A, 388, 29
Popping G., Somerville R. S., Trager S. C., 2014, MNRAS, 442, 2398
Roberts M. S., 1975, Radio Observations of Neutral Hydrogen in Galaxies, Sandage A., Sandage M., Kristian J., eds., the University of Chicago Press, p. 309
Robotham A. S. G., Obreschkow D., 2015, Publications of the Astronomical Society of Australia, 32, e033
Roychowdhury S., Chengalur J. N., Begum A., Karachentsev I. D., 2010, MNRAS, 404, L60
Roychowdhury S., Chengalur J. N., Chiboucas K., Karachentsev I. D., Tully R. B., Kaisin S. S., 2012, MNRAS, 426, 665

Roychowdhury S., Chengalur J. N., Kaisin S. S., Karachentsev I. D., 2014, MNRAS, 445, 1392
Roychowdhury S., Chengalur J. N., Karachentsev I. D., Kaisina E. I., 2013, MNRAS, 436, L104
Roychowdhury S., Chengalur J. N., Shi Y., 2017, A&A, 608, A24
Roychowdhury S., Huang M.-L., Kauffmann G., Wang J., Chengalur J. N., 2015, MNRAS, 449, 3700
Salpeter E. E., 1955, ApJ, 121, 161
Schlafly E. F., Finkbeiner D. P., 2011, ApJ, 737, 103
Schmidt M., 1959, ApJ, 129, 243
Schruba A. et al., 2011, AJ, 142, 37
Schruba A. et al., 2012, AJ, 143, 138
Seth A. C., Dalcanton J. J., de Jong R. S., 2005, AJ, 129, 1331
Shetty R., Kelly B. C., Rahman N., Bigiel F., Bolatto A. D., Clark P. C., Klessen R. S., Konstandin L. K., 2014, MNRAS, 437, L61
Shi Y., Helou G., Yan L., Armus L., Wu Y., Papovich C., Stierwalt S., 2011, ApJ, 733, 87
Staveley-Smith L. et al., 1996, PASA, 13, 243
Tonry J. L., Dressler A., Blakeslee J. P., Ajhar E. A., Fletcher A. B., Luppino G. A., Metzger M. R., Moore C. B., 2001, ApJ, 546, 681
Tosi M., Sabbi E., Bellazzini M., Aloisi A., Greggio L., Leitherer C., Montegriffo P., 2001, AJ, 122, 1271
Tully R. B., Fisher J. R., 1988, Catalog of Nearby Galaxies
Tully R. B. et al., 2006, AJ, 132, 729
Tully R. B., Shaya E. J., Karachentsev I. D., Courtois H. M., Kocevski D. D., Rizzi L., Peel A., 2008, ApJ, 676, 184
Vaduvescu O., McCall M. L., 2008, A&A, 487, 147
Vaduvescu O., McCall M. L., Richer M. G., Fingerhut R. L., 2005, AJ, 130, 1593
Vaduvescu O., Richer M. G., McCall M. L., 2006, AJ, 131, 1318
Wang J. et al., 2017, MNRAS, 472, 3029
Warren B. E., Jerjen H., Koribalski B. S., 2006, AJ, 131, 2056
Warren B. E., Jerjen H., Koribalski B. S., 2007, AJ, 134, 1849
Weisz D. R. et al., 2012, ApJ, 744, 44
Wong O. I., Meurer G. R., Zheng Z., Heckman T. M., Thilker D. A., Zwaan M. A., 2016, MNRAS, 460, 1106
Wyder T. K. et al., 2009, ApJ, 696, 1834
Young T., Jerjen H., López-Sánchez Á. R., Koribalski B. S., 2014, MNRAS, 444, 3052

Table 1. Table listing the externally obtained properties required to compute the surface densities for the KRDJ08 and YJLK14 NIR samples. The Table is arranged as follows: Column 1 - Galaxy name; Columns 2 and 3 - RA and DEC; Columns 4 - Morphology, using the classification scheme by de Vaucouleurs et al. (1991); Columns 5 and 6 - the radial distance in Mpc and the derivation method respectively. Note that obtained values have been rounded to the nearest decimal place since distance derivation methods are typically no more accurate than 10%; Column 7 - FUV flux, Column 8 - the 24μm luminosity; Column 9 - the H I flux; Column 10 - the B-band galactic extinction; Column 11 - the total observed luminosity in the B-band; Column 12 - B-H colour corrected for extinction (or the B-Ks data for the MVPB12 sample). Quantities are carefully cited in the caption for the KRDJ08 and YJLK14 samples. For the MVPB12 sample, their values have been taken as is and when available (such as distance modulus, H I fluxes, extinctions etc). The authors did not, however compile a list of B-band magnitudes, which we require in our computation of $R_{26.5,eq}$. Instead, we obtained them using the de Vaucouleurs et al. (1991) RC3 catalogue. Similarly, the quantities calculated for Kennicutt (1998) and Tully & Fisher (1988) cross correlated galaxies are not presented but these data can be made available upon request. References: ***Distance*** (a) Karachentsev et al. (2002a), (b) Karachentsev et al. (2003b), (c) Karachentsev et al. (2006), (d) Karachentsev et al. (2007), (e) Karachentsev, Makarov & Kaisina (2013), (f) Tully et al. (2006), (g) Tully et al. (2008), (h) Karachentsev et al. (2003a), (i) Karachentsev et al. (2002b), (j) Karachentsev et al. (2000), (k) Seth, Dalcanton & de Jong (2005), (l) Roychowdhury et al. (2012), (m) Cannon et al. (2003) , (n) Grisé et al. (2008), (o) Tosi et al. (2001), (p) Tonry et al. (2001), (q) Dalcanton et al. (2009); ***UV-band*** (a) *GALEX*, (b) Lee et al. (2011); ***B-band*** (a) de Vaucouleurs et al. (1991), (b) Lauberts & Valentijn (1989), (c) Karachentsev, Makarov & Kaisina (2013), (d) Metcalfe, Godwin & Peach (1994), (e) Parodi, Barazza & Binggeli (2002), (f) Jerjen, Freeman & Binggeli (2000), (g) Warren, Jerjen & Koribalski (2007), (h) Karachentsev et al. (2004), (i) Warren, Jerjen & Koribalski (2006), (j) Kouwenhoven et al. (2007), (k) Roychowdhury et al. (2012); ***H* I Flux**, (a) Doyle et al. (2005), (b) Begum et al. (2008), (c) Bouchard et al. (2005). For references pertaining to the MVPB12 data, the reader should consult their study.

Galaxy Name	RA (J2000)	DEC (J2000)	Type	D [Mpc]	Method	m_{FUV} [mag]	L(24μm) [erg s^{-1}]	FH I [Jy km s^{-1}]	A_B [mag]	m_B [mag]	$B-H$ [mag]
(1)	(2)	(3)	(4)	(5)	(6)	(7)	(8)	(9)	(10)	(11)	(12)
YJLK14											
AM1321-304	13 24 36.0	−30 58 20	10	4.6[a]	TRGB	18.8[a]	-	1.6[b]	0.25	16.7[d]	3.2
CEN06	13 05 02.1	−40 04 58	10	5.8[d]	TRGB	-	-	5.1[a]	0.37	17.7[f]	2.9
ESO149-G003	23 52 02.8	−52 34 39	10	5.9[a]	TF	15.7[b]	38.67	6.9[h]	0.05	15.1[b]	1.9
ESO199-G007	02 58 04.1	-49 22 57	10	6.6	h	17.9[a]	-	2.1[a]	0.08	16.4[b]	2.1
ESO222-G010	14 35 03.0	-49 25 18	10	5.8[e]	TF	-	-	7.0[a]	0.8	16.3[h]	3.2
ESO223-G009	15 01 08.5	-48 17 33	10	6.5[d]	TRGB	-	-	101.3[a]	0.94	13.8[h]	1.9
ESO252-IG001	04 56 58.7	-42 48 14	10	7.2[e]	TF	-	-	10.9[a]	0.05	14.4[a]	1.2
ESO269-G058	13 10 32.9	-46 59 27	9	3.8[d]	TRGB	17.2[a]	-	5.3[a]	0.39	13.3[a]	3.2
ESO272-G025	14 43 25.5	-44 42 19	10	5.9[a]	h	-	-	6.9[a]	0.58	14.8[b]	2.6

Table 2. Table listing the computed quantities for the NIR catalogue galaxies, and is arranged as follows : Column 1 - Name, Column 2 - $L(FUV)_{\rm corr}$, Column 3 - $\dot{M}_*$, Column 4 - $M_{\rm H\,I}$, Column 5 - $R_{26.5,eq}$, Column 6 - $\Sigma_{\rm H\,I}$, Column 7 - $\Sigma_{\rm SFR}$.

Galaxy Name	$L(FUV)_{\rm corr}$ [erg s^{-1}]	$\dot{M}_*$ [$M_\odot$ yr^{-1}]	$M_{\rm H\,I}$ [$M_\odot$]	$R_{26,eq}$ [pc]	$\Sigma_{\rm H\,I}$ log[$M_\odot$ pc^{-2}]	Σ_{SFR} log[$M_\odot$ yr^{-1} Kpc^{-2}]
YJLK14						
AM0106-382	-	-	-	1222		
CEN06	-	-	7.6	761	1.16	-
ESO149-G003	41.24	-1.90	7.8	1761	0.22	-3.44
ESO199-G007	40.48	-2.67	7.3	1476	0.07	-3.93
ESO222-G010	-	-	7.7	1708	0.66	-
ESO223-G009	-	-	9.0	3132	1.37	-
ESO252-IG001	-	-	8.1	1839	0.84	-
ESO269-G058	40.67	-2.48	7.3	1801	0.08	-3.66
ESO272-G025	-	-	7.7	1873	0.16	-